TrkB signaling in parvalbumin-positive interneurons is critical for gamma-band network synchronization in hippocampus

Kang Zheng[a,b], Juan Ji An[c], Feng Yang[a], Weifeng Xu[d], Zhi-Qing David Xu[b], Jianyoung Wu[d], Tomas G. M. Hökfelt[b,1], André Fisahn[e], Baoji Xu[c], and Bai Lu[f,1]

[a]Gene, Cognition and Psychosis Program, National Institute of Mental Health, National Institutes of Health, Bethesda, MD 20892-3714; [b]Department of Neuroscience, Karolinska Institutet, SE-17177 Stockholm, Sweden; Departments of [c]Pharmacology and [d]Neuroscience, Georgetown University, Washington, DC 20057; [e]Neuronal Oscillations Laboratory, Department of Neurobiology, Care Sciences and Society, KI-Alzheimer's Disease Research Center, Karolinska Institutet, SE-14186 Stockholm, Sweden; and [f]R&D China, GlaxoSmithKline, Pudong, Shanghai 201203, China

Contributed by Tomas G. M. Hökfelt, September 7, 2011 (sent for review February 13, 2011)

Although brain-derived neurotrophic factor (BDNF) is known to regulate circuit development and synaptic plasticity, its exact role in neuronal network activity remains elusive. Using mutant mice (TrkB-PV$^{-/-}$) in which the gene for the BDNF receptor, tyrosine kinase B receptor (*trkB*), has been specifically deleted in parvalbumin-expressing, fast-spiking GABAergic (PV+) interneurons, we show that TrkB is structurally and functionally important for the integrity of the hippocampal network. The amplitude of glutamatergic inputs to PV+ interneurons and the frequency of GABAergic inputs to excitatory pyramidal cells were reduced in the TrkB-PV$^{-/-}$ mice. Functionally, rhythmic network activity in the gamma-frequency band (30–80 Hz) was significantly decreased in hippocampal area CA1. This decrease was caused by a desynchronization and overall reduction in frequency of action potentials generated in PV+ interneurons of TrkB-PV$^{-/-}$ mice. Our results show that the integration of PV+ interneurons into the hippocampal microcircuit is impaired in TrkB-PV$^{-/-}$ mice, resulting in decreased rhythmic network activity in the gamma-frequency band.

gamma oscillations | synaptic transmission | Cre recombinase | dendrite | slice

Tyrosine kinase B receptor (TrkB), the cognate receptor for brain-derived neurotrophic factor (BDNF) and neurotrophin-4, mediates key signaling events that control many aspects of neuronal development and function (1–4), including the maturation of parvalbumin-positive (PV+) interneurons in the hippocampal microcircuit. BDNF is preferentially synthesized in, and secreted from glutamatergic neurons, whereas *trkB* is expressed in both glutamatergic and γ-aminobutyric acid (GABA)-ergic neurons in hippocampus (5). Among cortical interneurons, PV+ interneurons express *trkB* abundantly (6). This anatomical organization of the BDNF signaling components and the known importance of feedback and feedforward communication between principal cells and interneurons (7–11) suggest a potential role for TrkB signaling in modulating neuronal network function.

Rhythmic activity in cortical networks is important for the formation of neuronal assemblies (12–14). Of particular interest is rhythmic network activity in the gamma-frequency band (30–80 Hz, gamma oscillations) (15–17). Gamma oscillations are a result of the synchronized electrical activity of the neurons within a network and are thought to be important for temporal encoding, binding of sensory features, and memory storage and retrieval (18–22). Moreover, gamma oscillations are altered in several brain disorders, such as Alzheimer's disease (23–25), schizophrenia (24, 26–31), and epilepsy (24, 32, 33). Gamma oscillations are exquisitely susceptible to modulation of the cellular and synaptic mechanisms underlying the rhythmic activity. Fast-spiking PV+ interneurons are the main recipient of recurrent glutamatergic innervations in the hippocampal circuitry, and their role in gamma-frequency synchronization in cortical and hippocampal networks is well-established (34, 35). Despite extensive knowledge of the role of BDNF-TrkB signaling in neuronal development and synaptic function, the question of how BDNF might modulate and control rhythmic activity has so far not been answered.

To determine whether BDNF regulates synchronized network activity through PV+ interneurons (36, 37), we used a mutant mouse line, in which the *trkB* gene has been selectively ablated in PV+ interneurons. By inducing gamma oscillations in the hippocampal slice preparation with the muscarinic acetylcholine receptor agonist carbamoylcholine (CCh), we found that the power of gamma oscillations was dramatically reduced in the hippocampal area CA1 of mutant mice compared with control (Ctr) littermates. Morphological analysis and concomitant whole-cell patch-clamp and extracellular field recordings were used to determine, whether the decrease in gamma oscillation power was caused by morphological and/or functional alterations in PV+ interneurons. We also showed that the removal of TrkB signaling leads to a desynchronization and overall reduction in frequency of action potentials generated in PV+ interneurons, which is consistent with a reduction in gamma oscillation power. Taken together, our results demonstrate a critical role of BDNF-TrkB signaling in PV+ interneurons for hippocampal network synchrony in the gamma-frequency band.

Results

Ablation of the *trkB* Gene in PV+ Interneurons Using the PV-Cre Transgene. The calcium-binding protein PV serves as a marker of a subpopulation of GABAergic neurons with fast-spiking properties (38). To determine whether, and at what time point, PV+ interneurons express *trkB* during hippocampal development, we performed PV immunohistochemical staining on sections from *TrkB*$^{LacZ/+}$ knockin mice, in which β-galactosidase (β-gal) recapitulates the expression pattern of *trkB* (39). We found that the CA1 region starts to express *trkB* before postnatal day (P) 7 and PV between P7 and P14 (Fig. 1 *A* and *B*). In this brain region, *trkB* was expressed in nearly all PV+ interneurons (54 of 56) at P14 (Fig. 1B) and in all PV+ interneurons at P21 (Fig. 1*C*; 37 of 37) and at P28 (Fig. 1*D*; 24 of 24). Thus, CA1 PV+ interneurons express *trkB* during postnatal development and in adulthood.

Author contributions: K.Z., J.J.A., F.Y., Z.-Q.D.X., J.W., T.G.M.H., A.F., B.X., and B.L. designed research; K.Z. and J.J.A. performed research; K.Z., J.J.A., F.Y., W.X., J.W., T.G.M.H., B.X., and B.L. analyzed data; and K.Z., J.J.A., T.G.M.H., A.F., B.X., and B.L. wrote the paper.

The authors declare no conflict of interest.

Freely available online through the PNAS open access option.

[1]To whom correspondence may be addressed. E-mail: bai.b.lu@gsk.com or tomas.hokfelt@ki.se.

This article contains supporting information online at www.pnas.org/lookup/suppl/doi:10.1073/pnas.1114241108/-/DCSupplemental.

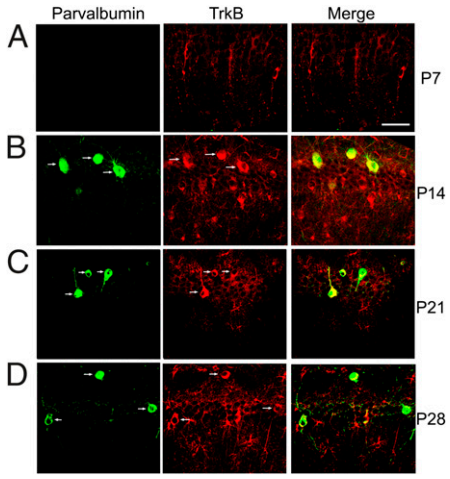

Fig. 1. Colocalization of TrkB and parvalbumin in the hippocampal CA1 region. Expression patterns of TrkB and parvalbumin in the hippocampal CA1 region were revealed by immunohistochemistry against parvalbumin and β-galactosidase in $TrkB^{LacZ/+}$ mice at P7 (*A*), P14 (*B*), P21 (*C*), and P28 (*D*). Arrows denote neurons expressing both parvalbumin and TrkB. (Scale bar: 50 μm.)

We used a *Cre* transgene driven by the PV promoter (*PV-Cre*) to delete the *trkB* gene in PV-expressing cells. To determine the efficiency of gene deletion mediated by *PV-Cre* in PV+ interneurons, we introduced this *PV-Cre* transgene into *Rosa26* reporter (*R26R*) mice, in which the *Rosa26* locus expresses β-galactosidase once Cre-mediated recombination has occurred (40). In *R26R/+;PV-Cre* mice, β-gal was expressed in the majority (22 of 31) of PV+ interneurons in hippocampal area CA1. Importantly, the Cre recombination activity was strictly confined to PV+ interneurons, because we did not detect any neurons that expressed β-gal but not PV (Fig. 2*A*).

We then crossed *PV-Cre* with floxed *trkB* (*fB*) mice to generate Ctr mice (*fB/fB*) and conditional *trkB* knockout mice (*fB/fB;PV-Cre*, also called TrkB-PV$^{-/-}$). Two approaches were used to determine whether the *trkB* gene was eliminated in PV+ interneurons of TrkB-PV$^{-/-}$ mice. First, a double-staining experiment was performed to detect TrkB mRNA by in situ hybridization (ISH) using fluorescence-labeled antisense oligonucleotides as a probe, and PV immunoreactivity by immunohistochemistry using an anti-PV antibody. We found that although many PV+ interneurons expressed TrkB mRNA in Ctr mice (Fig. 2*B*), there was hardly any TrkB signal in PV+ interneurons in TrkB-PV$^{-/-}$ mice (Fig. 2*C*). Importantly, *trkB* ISH signals were detectable in PV-negative cells, suggesting that the deletion of *trkB* gene was selective for PV+ interneurons. For the second approach, laser capture microdissection (LCM) was used to capture PV+ interneurons in hippocampal sections, followed by quantitative reverse-transcriptase PCR (qPCR) to measure TrkB mRNA levels in the captured tissue samples (Fig. 2*D*). We show that TrkB mRNA in CA1 PV+ interneurons isolated from TrkB-PV$^{-/-}$ mice was reduced to 19.7 ± 8.4% compared with those isolated from Ctr mice ($P < 0.05$; Fig. 2*E*). Together, these two approaches demonstrate a selective ablation of *trkB* gene in CA1 PV+ interneurons of TrkB-PV$^{-/-}$ mice. Interestingly, there was a 47.1 ± 4.9% reduction in the level of *PV* mRNA in CA1 PV+ interneurons isolated from TrkB-PV$^{-/-}$ mice compared with those from Ctr mice ($P < 0.05$; Fig. 2*E*), suggesting a reduction in PV expression even in PV+ cells.

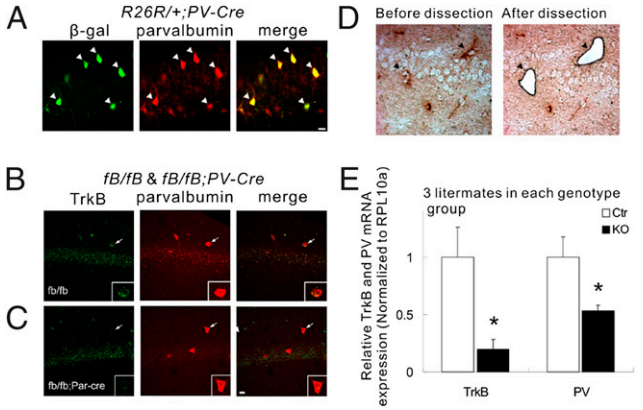

Fig. 2. Specific ablation of TrkB receptor in parvalbumin-positive interneurons in the hippocampal CA1 area. (*A*) Cell type-specific recombination of the Rosa26 reporter (R26R). The floxed *R26R* allele recombination was detected in the vast majority of PV+ neurons (white arrowheads) at P28, as revealed by immunohistochemistry against PV and β-galactosidase in *R26R/+;PV-Cre* mice. (*B* and *C*) Dual fluorescent in situ hybridization with probe for TrkB mRNA and immunohistochemistry with antibody against PV were carried out on brain sections from control mice (*fB/fB*) and *trkB* KO mice (*fB/fB;PV-Cre*). White arrows indicate the same neurons. Individual neurons are magnified in *Insets*. (*D*) Images of the CA1 region before and after LCM. The section was briefly stained with antibodies against PV (dark arrowheads). (*E*) qPCR using the mRNA isolated from the captured cells. Data are presented as means ± SEM. *$P < 0.05$. (Scale bars: 20 μm.)

Reduction in the Density of PV+ Interneurons and Their Dendrites. In agreement with a previous study (41), the vast majority of PV+ interneurons were found in the strata pyramidale (SP) and oriens (SO) of the hippocampal CA1–3 regions. We counted the number of PV+ interneurons within SO and SP of the CA1 area at different ages. The density of PV+ interneurons in the CA1 region was not different in TrkB-PV$^{-/-}$ mice versus Ctr mice at P14. However, the density was reduced by 16.3% at P28 (from 0.0295 to 0.0247 cell per μm^3; $P < 0.05$) and by 19.2% at 6 wk of age (from 0.0285 to 0.023 cell per μm^3; $P < 0.01$) (Fig. 3 *A* and *B*).

The dendritic morphology of PV+ interneurons, as measured by the density of PV+ neuropil, was examined in the CA1 region in P28 Ctr and TrkB-PV$^{-/-}$ mice after staining with the PV antibody. The dendrites of PV+ interneurons exhibited a 14.6 ± 5.9% reduction in length in strata radiatum (SR) ($P < 0.05$) and a 19.8 ± 4.9% reduction in SP ($P < 0.05$) in TrkB-PV$^{-/-}$ mice, respectively, compared with Ctr mice (Fig. 3 *C* and *D*; 4 littermates in each group). Taken together, deletion of the *trkB* gene elicited a modest effect on the dendrites and the number of PV+ interneurons in the hippocampal area CA1.

Decreased Excitatory Inputs to PV+ Interneurons and Inhibitory Inputs to Principal Neurons. The consequences of *trkB* ablation on the glutamatergic synaptic input onto PV+ interneurons were determined by recordings of miniature excitatory postsynaptic currents (mEPSCs). First, the PV+ interneurons were characterized based on their fast-spiking discharge pattern exhibited upon depolarization induced by current injection (Fig. 4 *A* and *B*) (38). The resting membrane potential and the number of depolarization-induced repetitive action potentials (AP) did not show a significant difference between Ctr and TrkB-PV$^{-/-}$ mice (Fig. 4*B*). Spontaneous mEPSCs were recorded in the fast-spiking interneurons in the presence of 2 μM tetrodotoxin (TTX) (Fig. 4*C*). The mEPSC amplitude in TrkB-PV$^{-/-}$ mice (17.61 ± 2.62 pA; $n = 13$ cells from 13 slices in six mice) was significantly reduced ($P < 0.01$) compared with Ctr mice (24.31 ± 4.66 pA; $n = 12$ cells from 12 slices in six mice) (Fig. 4*D*). However, the ablation of *trkB* did not seem to alter mEPSC frequency. Thus, the frequency of mEPSCs was 13.11 ± 4.22 Hz for Ctr and 16.4 ± 4.96 Hz for TrkB-PV$^{-/-}$ mice ($P = 0.078$; Fig. 4*E*). These results suggest that the ablation of *trkB* in PV+ interneurons pre-

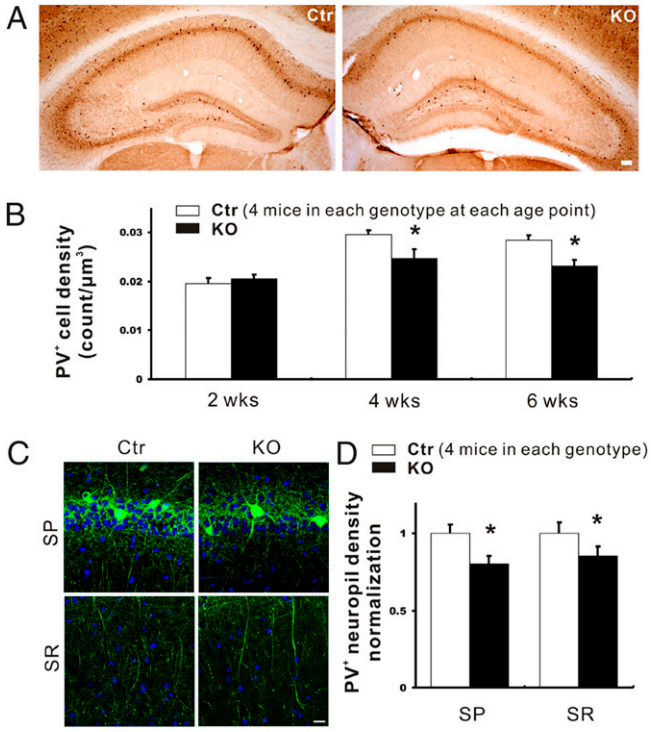

Fig. 3. PV+ cell number and neuropil density in the hippocampal CA1 area of conditional *TrkB* knockout (TrkB-PV$^{-/-}$, or KO) and control (Ctr) mice. (*A*) Representative images showing PV immunoreactivity in hippocampi of 4-wk-old Ctr and KO mice. (Scale bar: 100 μm.) (*B*) Density of PV+ cells in the CA1 regions of Ctr and KO mice at 2, 4, and 6 wk of age. (*C*) Representative fluorescence images showing immunoreactive neuropils in SP and SR of the CA1 area. (Scale bar: 50 μm.) (*D*) Density of PV-immunoreactive neuropil in the CA1 area. Data are presented as means ± SEM. *$P < 0.05$.

dominantly altered the postsynaptic AMPA receptor function rather than their presynaptic glutamatergic inputs (42).

We next asked whether the outputs of the PV+ interneurons in the TrkB-PV$^{-/-}$ mice were impaired. Spontaneous miniature inhibitory postsynaptic currents (mIPSCs), which reflect inhibitory inputs from GABAergic interneurons, including PV+ interneurons, were recorded in pyramidal neurons identified by their shape under an infrared-differential interference contrast microscope (43). All recordings were performed within the SP layer in the presence of 2 μM TTX, 25 μM 2R-amino-5-phosphonovaleric acid (Apv), and 25 μM 6-cyano-7-nitroquinoxaline-2,3-dione (CNQX) (Fig. 4*F*). The mIPSC amplitude showed no significant difference between Ctr mice (42.31 ± 11.32 pA; $n = 22$ cells from 22 slices in seven mice) and TrkB-PV$^{-/-}$ mice (36.59 ± 8.46 pA; $n = 20$ cells from 20 slices in seven mice; $P = 0.069$) (Fig. 4*G*). However, the ablation of *trkB* significantly reduced the mIPSC frequency from 19.2 ± 2.84 Hz in Ctr mice to 14.42 ± 1.91 Hz in TrkB-PV$^{-/-}$ mice ($P < 0.01$) (Fig. 4*H*). A large fraction of the total GABAergic cell population in the hippocampus is composed of the PV-expressing chandelier and basket cells, which contribute more substantially to the mIPSCs recorded in pyramidal neurons because of their largely somatic synaptic target profile. Moreover, *trkB* was selectively deleted in these PV+ interneurons but not in other GABAergic neurons. Thus, although we cannot exclude the possible contributions of other GABAergic interneurons, it is likely that the decrease in mIPSC frequency recorded in pyramidal neurons is due mostly to a decrease in GABA release from PV+ interneurons.

Decreased Power of Gamma Oscillations and Impaired Neuronal Synchrony. Changes in overall synaptic input and output of PV+ interneurons may alter hippocampal network activity. To test this possibility, CCh-induced extracellular gamma oscillations were recorded in the CA1 SR layer from acute hippocampal slices. In either Ctr or TrkB-PV$^{-/-}$ hippocampal slices, bath application of CCh (25 μM) induced a persistent network rhythm in the gamma-frequency band (peak frequency: 36.31 ± 3.06 Hz). As shown in Fig. 5*A*, the average peak power of the extracellular gamma oscillations in area CA1 was 5.80 ± 4.29e^{-5} in Ctr but 0.78 ± 0.29e^{-5} in TrkB-PV$^{-/-}$ slices. We next calculated power spectra and integral power for 20–80 Hz frequency range for 60-s-long recording segments as described in *Materials and Methods*. Both gamma oscillation power and power area were significantly reduced in area CA1 of TrkB-PV$^{-/-}$ slices compared with Ctr slices (Fig. 5 *B* and *C*). Specifically, the gamma band power recorded in TrkB-PV$^{-/-}$ slices was 3.986 ± 0.998e^{-5} mV^2 (five slices from five mice), compared with 17.81 ± 7.883e^{-5} mV^2 in Ctr slices (six slices from six mice; $P < 0.01$; Fig. 5*C*). There was no significant change in the oscillation peak frequency (TrkB-PV$^{-/-}$: 36.316 ± 3.058 Hz; Ctr: 36.031 ± 2.9 Hz; Fig. 5*D*).

To investigate the mechanism underlying the observed reduction of gamma oscillation amplitude and power, whole-cell patch clamp recordings of PV+ interneurons were performed concomitantly with extracellular field recordings of ongoing gamma oscillations (Fig. 6 *A* and *B*). Both in Ctr and TrkB-PV$^{-/-}$ recordings, the majority of action potentials occurred tightly phase-locked (phase angle π/4) shortly after the positive peak of the field oscillation, which was defined as phase angle 0° (Fig. 6 *C* and *F*). Although the peak phase angle in recordings from Ctr and TrkB-PV$^{-/-}$ cells was the same, the overall number of action potentials per gamma oscillation cycle generated by PV+ interneurons was significantly lower in TrkB-PV$^{-/-}$ mice (0.541 ± 0.131; $n = 6$ slices from six mice) compared with Ctr mice (0.992 ± 0.14; $n = 6$ slices from six mice; $P < 0.01$) (Fig. 6*E*), resulting in a relative desynchronization.

Discussion

Previous in vitro and in vivo studies have shown that the synaptic connection between pyramidal cells and PV+ interneurons, both locally and interregionally, is crucial for the emergence of gamma oscillations in CA1 (10, 44). Although BDNF-TrkB signaling is known to regulate synaptic formation and transmission tone between glutamatergic principal neurons and interneurons (1–4, 11), its specific role in network function remains unclear. Using the TrkB-PV$^{-/-}$ mice, in which the *trkB* gene has been specifically deleted in PV+ interneurons, we show that BDNF-TrkB signaling in PV+ interneurons is critical for the gamma band rhythmic activity in the hippocampal network.

The TrkB-PV$^{-/-}$ genotype littermates have a relatively normal PV+ interneuron population during early developmental stages, and the reduction of PV+ interneuron density was only found after P14. Given that *trkB* gene was not deleted in PV+ interneurons until after P14, the PV+ interneuron circuit development should be relatively normal. In young adults (4 or 6 wk old), there was a mild reduction in the density of PV+ neuropil, paralleling a small decrease in the number of PV+ cells. Laser capture of PV+ interneurons from hippocampal tissues combined with qPCR demonstrated that the TrkB mRNA expression is reduced, but not totally absent. Explanations include (*i*) the laser captured tissues may contain some nearby pyramidal cells, which also express *trkB*; (*ii*) TrkB mRNA may still be present in a small portion of PV cells that lacked Cre recombinase as shown by negative β-gal staining (Fig. 2*A*); and (*iii*) even in PV+ interneurons expressing Cre recombinase, the homologous recombination efficiency may not have been 100%, leaving some neurons with intact *trkB*. The moderate effect on PV+ in-

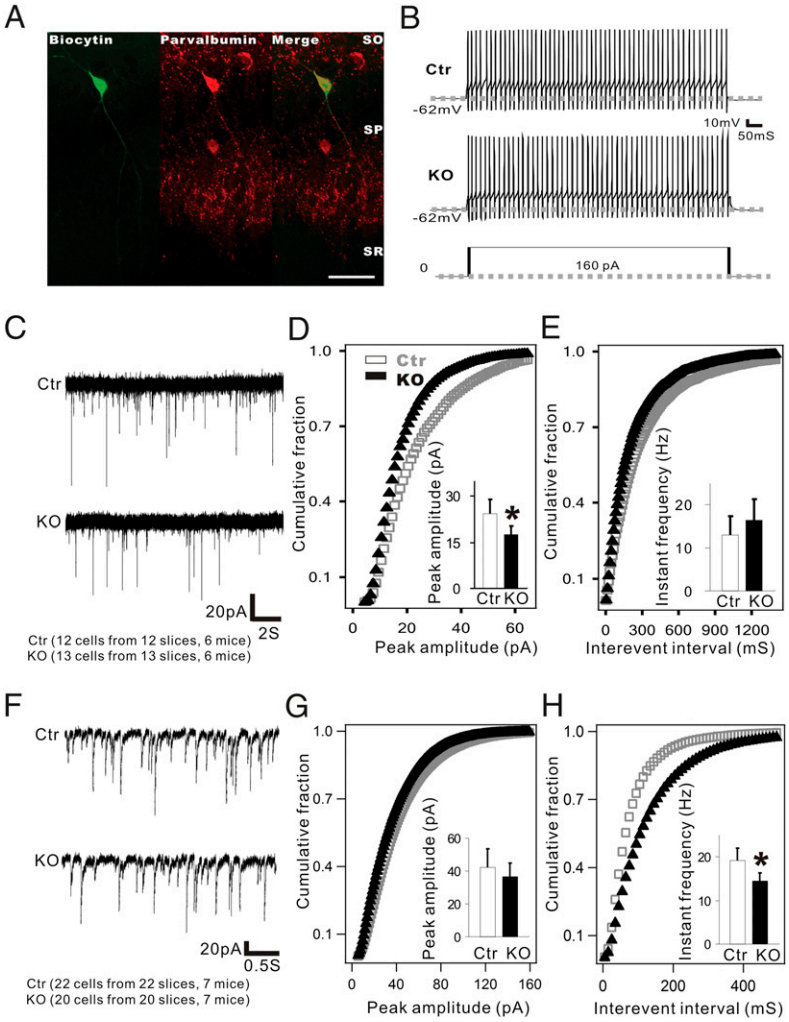

Fig. 4. Reduced mEPSC amplitude in PV+ interneurons and mIPSC frequency in pyramidal cells in TrkB-PV$^{-/-}$ (KO) mice. (*A*) Double immunohistochemistry of biocytin-labeled and recorded fast-spiking PV+ interneurons in the CA1 region. (Scale bar: 100 μm.) (*B*) Fast repetitive firing from the labeled cells from Ctr and KO mice. Action potentials were evoked by a 160-pA depolarizing current injected into neurons in the current clamp recording configuration. No differences in the excitability of fast-spiking cells were observed between Ctr and KO mice. (*C*) Sample traces of mEPSCs in fast-spiking neurons recorded from Ctr and KO mice. (*D* and *E*) Cumulative probability distributions were plotted against mEPSC amplitude and interevent interval in the fast-spiking neurons of Ctr and KO mice. The amplitude distribution of mEPSCs in mutant mice showed a left shift compared with control mice, indicating a reduction of mEPSCs amplitude in mutant mice. (*F–H*) Summary of mEPSCs amplitude and frequency was shown in both Ctr and KO mice, respectively. Data are presented as means ± SEM. *$P < 0.05$.

terneuron survival allows thorough analysis of the impact of *trkB* gene ablation in PV+ interneurons on neural network activity.

Ablation of the *trkB* gene in the PV+ interneurons resulted in two functional impairments. (*i*) The GABAergic neurons exhibited a decrease in the amplitude of mEPSCs without changing their excitability (Fig. 4 *B–E*). The most plausible interpretation of these data is the impairment of the postsynaptic capacity to respond to glutamatergic inputs from pyramidal neurons to the PV+ interneurons. (*ii*) There was a significant reduction in the frequency but not the amplitude of mIPSCs recorded from the pyramidal neurons (Fig. 4 *F–H*). This finding implied that the GABAergic inputs to the pyramidal neurons were impaired because of a reduction in either number of GABAergic synapse or probability of GABA release. In the hippocampus, a big portion of the total GABAergic cells are the PV+ interneurons, which form GABAergic synapses close to the cell body of pyramidal neurons and, therefore, contribute more substantially to the mIPSCs recorded in such neurons. Thus, the impairment in the GABAergic inputs to the pyramidal neurons is due most likely to a decrease in GABA release from PV+ interneurons, although we cannot exclude the possible contributions of other GABAergic interneurons.

In our whole-cell recordings of action potentials and concomitant field potential gamma oscillations, a reduction of overall number of action potentials generated by PV+ interneurons and a relative desynchronization were observed in PV+ interneurons in TrkB-PV$^{-/-}$ slices (Fig. 6). The reduced excitatory input resulting from lowered postsynaptic glutamate sensitivity in PV+ interneurons in TrkB-PV$^{-/-}$ slices may be one reason. A reduction in the number of action potentials may also reflect impairment in the inhibitory coupling between interneurons, further exacerbating the desynchronization of action potentials generated by PV+ interneurons. A direct consequence of this modification in firing characteristics is the observed reduction in gamma oscillation power in TrkB-PV$^{-/-}$ slices. Taken together, our data show that TrkB signaling is critical both for retaining physiological morphology and function of the hippocampal network. Given the importance of gamma

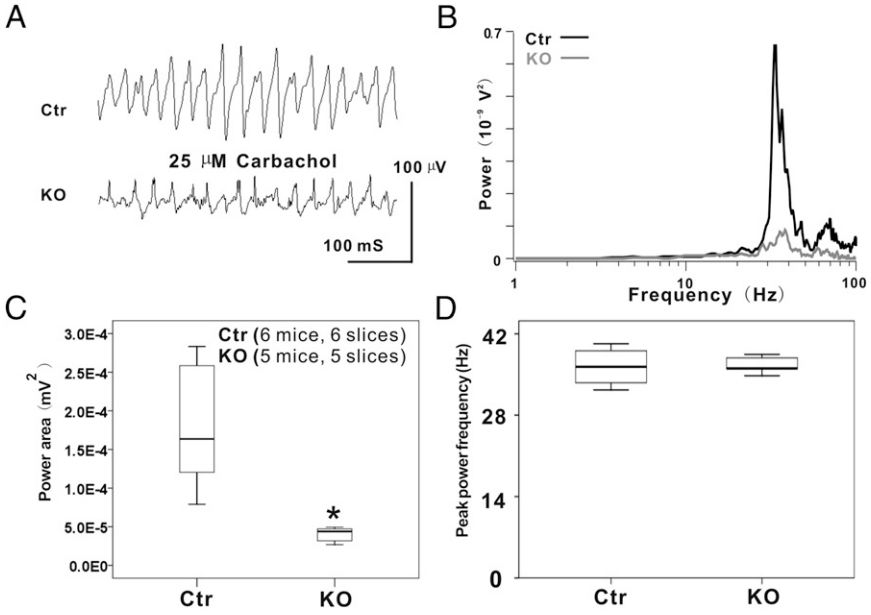

Fig. 5. Disrupted gamma oscillations in TrkB-PV$^{-/-}$ mice. (*A*) Representative traces of network oscillations were induced by 25 μM CCh in the middle to the distal one-third of the stratum radiatum of the hippocampal CA1 slices of both Ctr and KO mice. (*B*) Power spectra using a fast Fourier transform algorithm indicated a remarkable reduction of network oscillations in the CA1 region of KO mice compared with Ctr. The frequency of peaks appears to be at ≈40 Hz in both Ctr and KO animals. However, the peak amplitude was significantly smaller in KO mice than in Ctr mice. The power spectrum traces were averaged from six Ctr and five KO cases. (*C*) Dramatic reduction of the gamma oscillation power in KO mice compared with the Ctr. (*D*) Lack of significant change of the oscillation peak frequency in KO mice compared with Ctr mice. *$P < 0.05$.

oscillations for higher brain functions, our study also provides mechanistic insights into the importance of BDNF-TrkB signaling for hippocampal functions such as contextual memory and mood regulations. Finally, our findings support the view that genetic or environmental alteration of BDNF signaling may contribute to the abnormal circuit development or pathological network dynamics seen in neurological and psychiatric disorders.

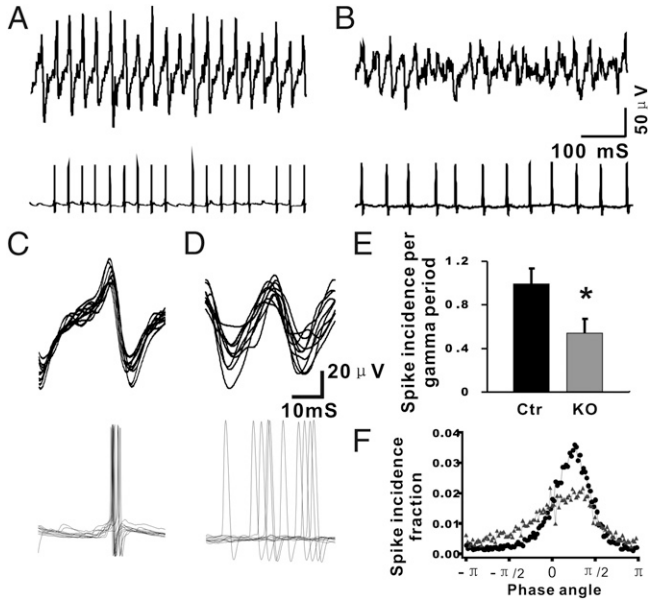

Fig. 6. Impaired firing phase distribution in fast-spiking interneurons of TrkB-PV$^{-/-}$ mice. (*A* and *B*) Examples showing simultaneous recordings of both extracellular gamma oscillations and PV+ interneuron action potentials in hippocampal area CA1, with Ctr and KO mice, respectively. (*C* and *D*) The data obtained from 10 continuous gamma cycles, and correlated spikes in Ctr and KO mice were pooled together to compare the phase angle of the APs. (*E*) The data were analyzed by averaging AP incidence per gamma cycle across 100 gamma cycles. The average AP incidence per gamma cycle in KO mice was significantly reduced compared with control mice. *$P < 0.05$. (*F*) The AP recorded in fast-spiking interneurons was wider in KO mice than in Ctr mice.

Materials and Methods

Animals. All procedures were approved by the National Institutes of Health (NIH) Animal Care and Use Committee and followed the NIH Guidelines ''Using Animals in Intramural Research.'' Conditional *trkB* knockouts (*fB/fB; PV-Cre*, or TrkB-PV$^{-/-}$) mice were generated by crossing *PV-Cre* with floxed *trkB* (*fB*) mice. The TrkB-PV$^{-/-}$ KO and *fB* Ctr littermates were identified by genotyping the floxed *trkB* and *Cre* sequences.

Physiological Recording. Recordings were performed by using horizontal hippocampal slices with 400-μm thickness from Ctr and KO mice (21–35 d old), in submerged recording chamber perfused with ACSF at 33 ± 1 °C.

Gamma Oscillations Analysis. The power spectra and integral power for 20–80 Hz frequency range were calculated for 60-s-long recording segments by using fast Fourier transformation in Clampfit 9.2 (Molecular Devices). The phase relationship between the neuronal spiking and the gamma oscillations was analyzed by calculating the phase of each spike relative to the oscillation cycle. Matlab functions (Hilbert and Angle) were applied to extract the phase information at any time [phase(t)].

Immunohistochemistry and in Situ Hybridization. Immunohistochemistry using coronal brain sections (50 μm thick) was performed as described (27). Fluorescent in situ hybridization using DIG-labeled probes was carried out as detailed (31). The *trkB* probe covered nucleotides 188–722 (GenBank accession no. X17647).

Measurement of Neuron Number and Dendrite Density. PV interneurons were counted after DAB staining in a double-blind designation. PV-IR dendrite density was measured by calculating the optical density of saturated confocal image, after staining with Alexa Fluor 488 secondary antibody (Invitrogen).

Staining of Frozen Tissue Sections, Laser Capture Microdissection, RNA Isolation, and Quantitative PCR Analysis. Hippocampal CA1 PV interneurons were fast immunostained as described (32). PV-IR neurons (300–400) were dissected out

with the Arcturus LCM system from Molecular Devices (33, 34). Total RNA was isolated from the captured PV interneurons by using Ambion RNAqueous Microkit (Ambion and Applied Biosystems) (35). First-strand cDNA was reverse-transcribed by using total RNA and Super-Script II (Invitrogen) according to the manufacturer's protocol. qPCR was performed by using Step-One thermal cycler (Applied Biosystems) with SYBR Green PCR master mix (Roche). Levels of TrkB and PV mRNAs were normalized over the RPL10a mRNA level in the same sample. Detailed methods are provided in *SI Materials and Methods*.

ACKNOWLEDGMENTS. We thank Dr. Robert F. Bonner (Section on Medical Biophysics, National Institute of Child Health and Human Development); Dr. Jaime Rodriguez-Canales and Mr. Jeffrey Charles Hanson (Laboratory of Pathology, National Cancer Institute); and Dr. Wen-Jun Gao (Department of Neurobiology and Anatomy, Drexel University College of Medicine) for providing technical help with laser capture microdissection. This work was supported by the Intramural Research Programs of the National Institute of Mental Health (to B.L.), Swedish Research Council (to T.G.M.H.), National Institutes of Health/Karolinska Institutet Collaborative Doctoral Program in Neuroscience (to T.G.M.H.), and National Institutes of Health Grant NS050596 (to B.X.).

1. Huang EJ, Reichardt LF (2003) Trk receptors: Roles in neuronal signal transduction. *Annu Rev Biochem* 72:609–642.
2. Lu B (2003) BDNF and activity-dependent synaptic modulation. *Learn Mem* 10:86–98.
3. Lu B (2003) Pro-region of neurotrophins: Role in synaptic modulation. *Neuron* 39: 735–738.
4. Nagappan G, Lu B (2005) Activity-dependent modulation of the BDNF receptor TrkB: Mechanisms and implications. *Trends Neurosci* 28:464–471.
5. Swanwick CC, Harrison MB, Kapur J (2004) Synaptic and extrasynaptic localization of brain-derived neurotrophic factor and the tyrosine kinase B receptor in cultured hippocampal neurons. *J Comp Neurol* 478:405–417.
6. Cellerino A, Maffei L, Domenici L (1996) The distribution of brain-derived neurotrophic factor and its receptor trkB in parvalbumin-containing neurons of the rat visual cortex. *Eur J Neurosci* 8:1190–1197.
7. Wang Y, Fujita I, Murayama Y (2000) Neuronal mechanisms of selectivity for object features revealed by blocking inhibition in inferotemporal cortex. *Nat Neurosci* 3: 807–813.
8. Galarreta M, Hestrin S (1999) A network of fast-spiking cells in the neocortex connected by electrical synapses. *Nature* 402:72–75.
9. Freund TF (2003) Interneuron Diversity series: Rhythm and mood in perisomatic inhibition. *Trends Neurosci* 26:489–495.
10. Csicsvari J, Jamieson B, Wise KD, Buzsáki G (2003) Mechanisms of gamma oscillations in the hippocampus of the behaving rat. *Neuron* 37:311–322.
11. Kohara K, et al. (2007) A local reduction in cortical GABAergic synapses after a loss of endogenous brain-derived neurotrophic factor, as revealed by single-cell gene knockout method. *J Neurosci* 27:7234–7244.
12. Singer W (1994) Time as coding space in neocortical processing: A Hypothesis. *Temporal Coding in the Brain*, eds Buzsáki G, et al., (Springer-Verlag, Berlin), pp 51–80.
13. Engel AK, Fries P, Singer W (2001) Dynamic predictions: Oscillations and synchrony in top-down processing. *Nat Rev Neurosci* 2:704–716.
14. Buzsáki G (2006) *Rhythms of the Brain* (Oxford University Press, New York), pp 136–174.
15. Gray CM, Singer W (1989) Stimulus-specific neuronal oscillations in orientation columns of cat visual cortex. *Proc Natl Acad Sci USA* 86:1698–1702.
16. Fries P, Nikolić D, Singer W (2007) The gamma cycle. *Trends Neurosci* 30:309–316.
17. Grosse-Wentrup M, Schölkopf B, Hill J (2011) Causal influence of gamma oscillations on the sensorimotor rhythm. *Neuroimage* 56:837–842.
18. Freeman W (1975) *Mass action in the nervous system: Examination of the neurophysiological basis of adaptive behavior through EEG* (Academic, New York), p 489.
19. Singer W, Gray CM (1995) Visual feature integration and the temporal correlation hypothesis. *Annu Rev Neurosci* 18:555–586.
20. Rodriguez E, et al. (1999) Perception's shadow: Long-distance synchronization of human brain activity. *Nature* 397:430–433.
21. Tallon-Baudry C, Bertrand O (1999) Oscillatory gamma activity in humans and its role in object representation. *Trends Cogn Sci* 3:151–162.
22. Fries P (2005) A mechanism for cognitive dynamics: Neuronal communication through neuronal coherence. *Trends Cogn Sci* 9:474–480.
23. Ribary U, et al. (1991) Magnetic field tomography of coherent thalamocortical 40-Hz oscillations in humans. *Proc Natl Acad Sci USA* 88:11037–11041.
24. Uhlhaas PJ, Singer W (2006) Neural synchrony in brain disorders: Relevance for cognitive dysfunctions and pathophysiology. *Neuron* 52:155–168.
25. Stam CJ (2010) Use of magnetoencephalography (MEG) to study functional brain networks in neurodegenerative disorders. *J Neurol Sci* 289:128–134.
26. Spencer KM, et al. (2004) Neural synchrony indexes disordered perception and cognition in schizophrenia. *Proc Natl Acad Sci USA* 101:17288–17293.
27. Kwon JS, et al. (1999) Gamma frequency-range abnormalities to auditory stimulation in schizophrenia. *Arch Gen Psychiatry* 56:1001–1005.
28. Hajós M (2006) Targeting information-processing deficit in schizophrenia: A novel approach to psychotherapeutic drug discovery. *Trends Pharmacol Sci* 27:391–398.
29. Hong LE, et al. (2008) Sensory gating endophenotype based on its neural oscillatory pattern and heritability estimate. *Arch Gen Psychiatry* 65:1008–1016.
30. Uhlhaas PJ, Haenschel C, Nikolić D, Singer W (2008) The role of oscillations and synchrony in cortical networks and their putative relevance for the pathophysiology of schizophrenia. *Schizophr Bull* 34:927–943.
31. Uhlhaas PJ, Singer W (2010) Abnormal neural oscillations and synchrony in schizophrenia. *Nat Rev Neurosci* 11:100–113.
32. Dugladze T, et al. (2007) Impaired hippocampal rhythmogenesis in a mouse model of mesial temporal lobe epilepsy. *Proc Natl Acad Sci USA* 104:17530–17535.
33. Voss LJ, Sleigh JW, Barnard JP, Kirsch HE (2008) The howling cortex: Seizures and general anesthetic drugs. *Anesth Analg* 107:1689–1703.
34. Sohal VS, Zhang F, Yizhar O, Deisseroth K (2009) Parvalbumin neurons and gamma rhythms enhance cortical circuit performance. *Nature* 459:698–702.
35. Gulyás AI, Megías M, Emri Z, Freund TF (1999) Total number and ratio of excitatory and inhibitory synapses converging onto single interneurons of different types in the CA1 area of the rat hippocampus. *J Neurosci* 19:10082–10097.
36. Mann EO, Suckling JM, Hajos N, Greenfield SA, Paulsen O (2005) Perisomatic feedback inhibition underlies cholinergically induced fast network oscillations in the rat hippocampus in vitro. *Neuron* 45:105–117.
37. Klausberger T, Somogyi P (2008) Neuronal diversity and temporal dynamics: The unity of hippocampal circuit operations. *Science* 321:53–57.
38. Kawaguchi Y, Katsumaru H, Kosaka T, Heizmann CW, Hama K (1987) Fast spiking cells in rat hippocampus (CA1 region) contain the calcium-binding protein parvalbumin. *Brain Res* 416:369–374.
39. Xu B, et al. (2000) Cortical degeneration in the absence of neurotrophin signaling: Dendritic retraction and neuronal loss after removal of the receptor TrkB. *Neuron* 26: 233–245.
40. Soriano P (1999) Generalized lacZ expression with the ROSA26 Cre reporter strain. *Nat Genet* 21:70–71.
41. Mátyás F, Freund TF, Gulyás AI (2004) Immunocytochemically defined interneuron populations in the hippocampus of mouse strains used in transgenic technology. *Hippocampus* 14:460–481.
42. Bekkers JM, Richerson GB, Stevens CF (1990) Origin of variability in quantal size in cultured hippocampal neurons and hippocampal slices. *Proc Natl Acad Sci USA* 87: 5359–5362.
43. Hong EJ, McCord AE, Greenberg ME (2008) A biological function for the neuronal activity-dependent component of Bdnf transcription in the development of cortical inhibition. *Neuron* 60:610–624.
44. Fisahn A, Pike FG, Buhl EH, Paulsen O (1998) Cholinergic induction of network oscillations at 40 Hz in the hippocampus in vitro. *Nature* 394:186–189.